## **ELECTROCHEMISTRY**

# Solid electrolyte interphases for high-energy aqueous aluminum electrochemical cells

Qing Zhao<sup>1</sup>, Michael J. Zachman<sup>2</sup>\*, Wajdi I. Al Sadat<sup>3</sup>, Jingxu Zheng<sup>4</sup>, Lena F. Kourkoutis<sup>2,5</sup>, Lynden Archer<sup>1,4†</sup>

Electrochemical cells based on aluminum (Al) are of long-standing interest because Al is earth abundant, low cost, and chemically inert. The trivalent Al<sup>3+</sup> ions also offer among the highest volume-specific charge storage capacities (8040 mAh cm<sup>-3</sup>), approximately four times larger than achievable for Li metal anodes. Rapid and irreversible formation of a high-electrical bandgap passivating Al<sub>2</sub>O<sub>3</sub> oxide film on Al have, to date, frustrated all efforts to create aqueous Al-based electrochemical cells with high reversibility. Here, we investigate the interphases formed on metallic Al in contact with ionic liquid (IL)–eutectic electrolytes and find that artificial solid electrolyte interphases (ASEIs) formed spontaneously on the metal permanently transform its interfacial chemistry. The resultant IL-ASEIs are further shown to enable aqueous Al electrochemical cells with unprecedented reversibility. As an illustration of the potential benefits of these interphases, we create simple Al||MnO<sub>2</sub> aqueous cells and report that they provide high specific energy (approximately 500 Wh/kg, based on MnO<sub>2</sub> mass in the cathode) and intrinsic safety features required for applications.

Copyright © 2018
The Authors, some rights reserved; exclusive licensee
American Association for the Advancement of Science. No claim to original U.S. Government Works. Distributed under a Creative
Commons Attribution
NonCommercial
License 4.0 (CC BY-NC).

#### **INTRODUCTION**

The high cost and inherently poor safety of state-of-the-art lithium batteries are among the most important barriers to broad-based electrification of transportation (1, 2). The most recent report from the U.S. Environmental Protection Agency (EPA) shows that combustion of fossil fuels in transportation may be responsible for more than onequarter of all CO<sub>2</sub> emissions in the United States each year (3). New approaches are needed to develop electrical energy storage technology that moves beyond the cost and safety constraints that limit widespread acceptance of electrification in transportation. As the most abundant metallic element in Earth's crust, aluminum has been of interest because it is already a widely used commodity material in global commerce and can store up to three charge equivalents per mole of the metal. As a result, Al anodes offer among the highest volume-specific storage capacities (8040 mAh cm<sup>-3</sup>) in an inherently safe material (4–6). Previous efforts to realize rechargeable batteries that live up to the promise of low cost, intrinsic safety, and high-energy storage features associated with this chemistry have been largely unsuccessful because Al readily forms a high-bandgap passivating oxide coating that makes the metal electrochemically inert in electrolytes that preserve its cost and safety features. In particular, in aqueous electrolytes, the high potentials required to drive ion transport through the passivating oxide coating easily exceed the thermodynamic stability limits for water, resulting in continuous electrolyte degradation and hydrogen generation during battery recharge. As a consequence, until recently, most Al cells, such as Al-air (7) and Al-S (8) batteries, could not be recharged in

Previously, we reported that electrolytes based on the acidic ionic liquid (IL) melt aluminum chloride (AlCl<sub>3</sub>)–1-ethyl-3-methylimidazolium

chloride ([EMIm]Cl) provide a mechanism for overcoming oxide passivation of Al anodes and therefore enable rechargeable Al batteries (9) by pairing the metal with a metal oxide cathode. These findings have provided the basis for a growing body of research in which IL electrolytes have been used to create rechargeable Al batteries using other materials, such as graphite (10, 11), sulfur (12, 13), iodine (14), metal sulfides (15-17), and MXene (18), as the cathode. Although the role of the IL electrolyte is poorly understood, the acidic AlCl<sub>3</sub>-IL melt is thought to enable reversible stripping and plating of Al by forming AlCl<sub>4</sub> ions in the electrolyte, which react reversibly with the Al anode during battery discharge to create Al<sub>2</sub>Cl<sub>7</sub><sup>-</sup>. This means that AlCl<sub>4</sub><sup>-</sup> and Al<sub>2</sub>Cl<sub>7</sub><sup>-</sup> (i.e., not Al<sup>3+</sup>) are the electrochemically active species in the IL electrolyte. An additional benefit of the IL electrolyte solvent is its thermodynamic stability over a wider range of potentials than water, which, in principle, opens a path to rechargeable Al cells in which the metal is paired with a high-voltage cathode. The large size and complexity of the electrochemically active AlCl<sub>4</sub> and Al<sub>2</sub>Cl<sub>7</sub> ions have, in practice, introduced new complexity, frustrating all efforts to create suitably highcapacity cathode materials that can be used in rechargeable Al batteries (5). The highly corrosive and air-sensitive characteristics of the AlCl<sub>3</sub>-IL electrolytes provide additional impediments to progress most importantly reduced cell safety, increased complexity, and cost of battery design and manufacturing processes, all of which motivate interest in other types of electrolytes in which Al<sup>3+</sup> is the electrochemically active ion.

Conventional wisdom holds that corrosive electrolytes such as AlCl<sub>3</sub>-[EMIm]Cl (5) or alkali (NaOH) (7) are effective in Al batteries because they erode the passivating oxide film. The solid electrolyte interphases (SEIs) formed on the anodes in these cells have, to date, not been studied in detail. However, based on the importance of well-formed SEI in enabling reversible operations of lithium ion (19) and lithium metal batteries (20) in liquid electrolytes, we hypothesize that a detailed understanding of the SEI that AlCl<sub>3</sub>-[EMIm]Cl forms on Al may provide a strategy for designing other electrolytes for the Al anode. Here, we study the interphases formed on Al electrodes in AlCl<sub>3</sub>-[EMIm] Cl and find that a tightly bound, IL-enriched film spontaneously forms on the interface that appears to simultaneously erode the Al<sub>2</sub>O<sub>3</sub> oxide film and protect the metal against subsequent formation of the oxide. Furthermore, we find that this interface can be transferred, essentially

<sup>&</sup>lt;sup>1</sup>Robert Frederick Smith School of Chemical and Biomolecular Engineering, Cornell University, Ithaca, NY 14853, USA. <sup>2</sup>School of Applied and Engineering Physics, Cornell University, Ithaca, NY 14853, USA. <sup>3</sup>Research & Development Center, Saudi Aramco, Dhahran 31311, Saudi Arabia. <sup>4</sup>Department of Materials Science and Engineering, Cornell University, Ithaca, NY 14853, USA. <sup>5</sup>Kavli Institute at Cornell for Nanoscale Science, Cornell University, Ithaca, NY 4853, USA.

<sup>\*</sup>Present address: Center for Nanophase Materials Sciences, Oak Ridge National Laboratory, Oak Ridge, TN 37831, USA.

<sup>†</sup>Corresponding author. Email: laa25@cornell.edu

intact, when an  $AlCl_3$ -IL-treated Al substrate is used in conjunction with aqueous electrolytes. The treated electrodes exhibit exceptional reversibility in both symmetric Al cells and full cells, in which Al is paired with a  $MnO_2$  cathode.

#### **RESULTS**

#### Design interphase for aqueous Al batteries

The structure and composition of the interface formed on an Al electrode in an AlCl<sub>3</sub>-IL electrolyte (TAl electrode) were interrogated using attenuated total reflection-Fourier transform infrared spectroscopy (ATR-FTIR), scanning electron microscopy (SEM), energydispersive x-ray spectroscopy (EDX), and x-ray photoelectron spectroscopy (XPS). Compared with pure Al, the surface of TAl is enriched with organic functional groups (Fig. 1A). In addition to the presence of C=N and C-H groups that are also abundant in the pristine IL electrolyte, a large enhancement in the C=C functional group and emergence of species containing the C=O group are detected on TAl. These observations are accompanied by the appearance of a stable film on the TAI surface. In addition, infrared vibration modes associated with the imidazolium ring (1100 to 600 cm<sup>-1</sup>) in the IL (21) largely disappear upon treatment, which indicates that the IL electrolyte is chemically transformed at the Al interface (Fig. 1A). XPS analysis of the pristine Al and TAl provides additional insights into the surface chemical features of TAl. Results in Fig. 1B, for example, show that even after polishing, Al<sub>2</sub>O<sub>3</sub> still dominates the surface chemistry of the pristine Al. In contrast, the Al<sub>2p</sub> XPS spectra of TAl substrate reveal that a composite with higher binding energy, which can be attributed to

an Al salt, likely AlCl<sub>3</sub>, dominates. This is confirmed by the  $\rm Cl_{2p}$  XPS spectra, because the binding energy of  $\rm Cl_{2p}$  located at about 199 eV is consistent with a valence of -1 (Fig. 1C). The  $\rm N_{1s}$  XPS spectra also show that the interface of the TAl is enriched in nitrogencontaining species. The sharp peak at 401 eV can be used to unequivocally identify the presence of imidazole ions (Fig. 1D). Compared with a pristine polished Al surface (Fig. 1E), the surface topography of TAl is obviously smoother (Fig. 1F). From the cross-section view imaged by SEM, an interfacial layer is observed on the Al substrate. EDX analysis of the layer shows that it is rich in the elements Al, Cl, and N (Fig. 1G and fig. S1).

A good SEI for Al must not only prevent the formation of the passivating Al<sub>2</sub>O<sub>3</sub> coating but also enable fast charge transport at the electrolyte/electrode interface and reversible deposition of Al during electrochemical cycling. To evaluate charge transport characteristics and stability of the interface formed on the TAl electrode, the reversibility of Al plating and stripping processes was investigated in aqueous electrolytes containing aluminum sulfate [Al<sub>2</sub>(SO<sub>4</sub>)<sub>3</sub>] and aluminum trifluoromethanesulfonate [Al(CF<sub>3</sub>SO<sub>3</sub>)<sub>3</sub>] salts at concentrations ranging from 1 m to 5 m. Results reported in Fig. 2A indicate that the electrolytes generally have high ionic conductivity. Specifically, at 20°C, conductivity values of 24.6, 49.6, 27.5, 22.8, and 7.26 mS/cm are recorded for the 1 m  $Al_2(SO_4)_3$  electrolyte and the 1 m, 2 m, 3 m, and 5 m Al(CF<sub>3</sub>SO<sub>3</sub>)<sub>3</sub> electrolytes, respectively. It is also apparent from the plot that the ionic conductivities of all electrolytes are above 1 mS/cm at temperatures in the range of −10° to 60°C. The crucial role interface chemistry plays in the reversibility of ion transport to the electrode is readily seen by comparing the charge-transfer resistance

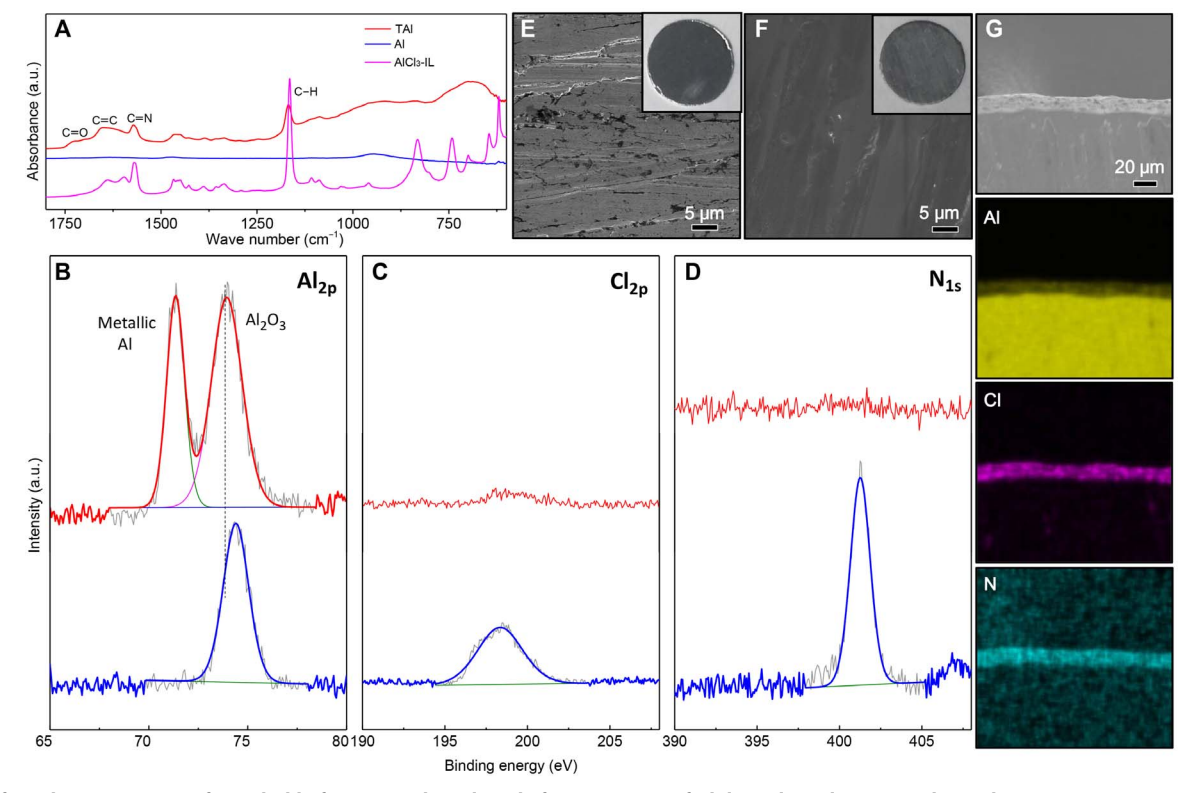


Fig. 1. Surface characterization of metal Al before (named as Al) and after treatment of AlCl<sub>3</sub>-IL electrolyte (named as TAl). (A) ATR-FTIR spectra of Al and TAl foil. XPS spectra of (B)  $Al_{2p}$ , (C)  $Al_{2p}$ , and (D)  $Al_{2p}$ , and (E)  $Al_{2p}$ , and (E)

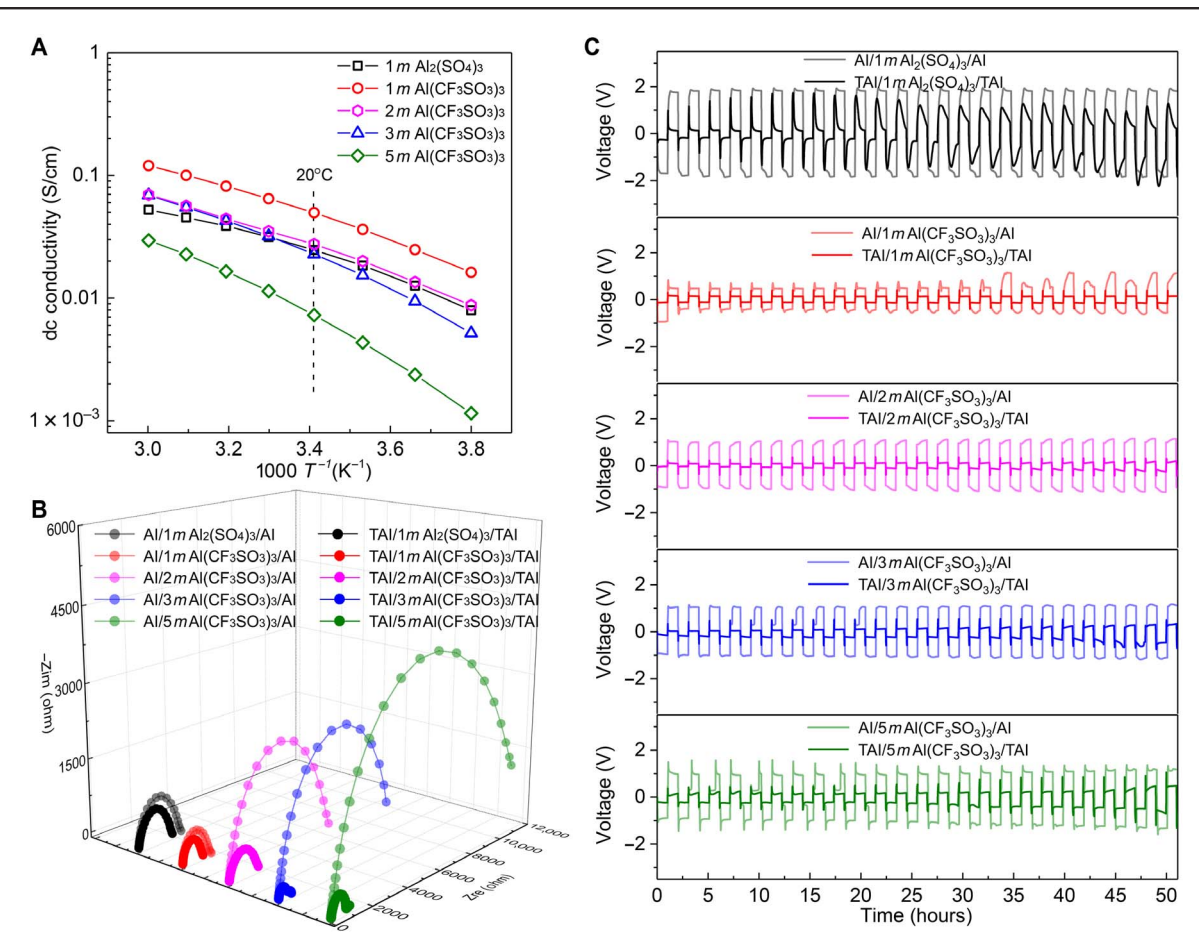


Fig. 2. Electrochemical studies of aqueous electrolytes in Al batteries. (A) dc ionic conductivity of aqueous  $Al_2(SO_4)_3$  electrolyte and  $Al(CF_3SO_3)_3$  electrolytes with varying different concentrations as a function of temperature. (B) Electrochemical impedance spectroscopy (EIS) of symmetric Al batteries using different Al anodes and electrolytes. (C) Symmetric Al battery tests using Al and TAl coupled with different electrolytes. The current density is 0.2 mA cm<sup>-2</sup>. Each cycle contains the discharge process for 1 hour and the charge process for 1 hour, separately.

for the pristine and TAl electrodes. As shown in Fig. 2B, the charge-transfer resistances of symmetric pristine Al cells using aqueous electrolytes are enormous, as high as 5500 ohms and more than 10,000 ohms for the 2 m and 5 m Al(CF<sub>3</sub>SO<sub>3</sub>)<sub>3</sub> electrolytes, respectively. Whatever the conductivity of the electrolytes, these high charge-transfer resistances make the pristine Al electrode unviable as a candidate for a rechargeable aqueous Al electrochemical cell. In contrast, the figure shows that much smaller charge-transfer resistances are observed in symmetric cells based on TAl electrodes, underscoring the importance of the interfacial layer on charge transfer to the electrode. The results show that the differences between charge-transfer resistance of pristine Al and TAl electrodes are reduced in aqueous electrolytes with lower salt concentrations, indicating that a proper concentration is needed to keep the interface durable.

Comparison of the overpotential for Al stripping/plating in cells based on pristine Al and TAl electrodes (Fig. 2C) shows that cells using the  $Al_2(SO_4)_3$  electrolyte and a pristine Al electrode exhibit extremely high overpotentials. The potential gap between plating and stripping is about 4 V. For comparison, the gap is 1 V for 1 m Al(CF<sub>3</sub>SO<sub>3</sub>)<sub>3</sub> electrolytes and about 2.0 V for 5 m Al(CF<sub>3</sub>SO<sub>3</sub>)<sub>3</sub> electrolytes when pristine Al electrodes are used. These high potential gaps stand in sharp contrast to those evident in the 1 m and 2 m Al(CF<sub>3</sub>SO<sub>3</sub>)<sub>3</sub> electrolytes using TAl electrodes, where the gap between plating and stripping is

about 0.2 V. The gap increases with increasing salt concentration in the electrolytes, but is seen to remain relatively low even at high current densities (fig. S2), confirming that a proper concentration associated with high thermodynamic stability is needed to stabilize the artificial SEI (ASEI). Even in a noncorrosive organic electrolyte [1 m Al(CF<sub>3</sub>SO<sub>3</sub>)<sub>3</sub> in dimethoxyethane (DME)], the TAl also exhibits much lower polarization than the Al anode (fig. S3). These results confirm that the interphases formed on the TAI electrode are favorable for ion transport and that the chemistry of the electrolyte salt used in an aqueous electrolyte plays an additional beneficial role. Results reported in fig. S4 show that the salt plays an additional important role in the high-voltage stability of the cell. All the electrolytes containing Al(CF<sub>3</sub>SO<sub>3</sub>)<sub>3</sub> salt display increased high-voltage electrochemical stability (in some cases by more than 2 V) than the corresponding electrolytes based on 1 m  $Al_2(SO_4)_3$ (~1.5 V). The concentration of Al(CF<sub>3</sub>SO<sub>3</sub>)<sub>3</sub> is also found to have a significant influence on the potential range over which the aqueous electrolyte is electrochemically stable. The stability can be improved further by increasing the concentration of Al(CF<sub>3</sub>SO<sub>3</sub>)<sub>3</sub>. This phenomenon is thought to reflect changes in the interface composition and in the interaction strength between salt and water at high salt concentrations (22–24), observations that are partially confirmed by ATR-FTIR spectra (fig. S5). In combination with results from the previous surface characterizations, we propose that the SEI on Al is composed of a mixture of N-rich organic compounds derived from decomposition of the IL and inorganics derived from AlCl<sub>3</sub>. The organic surface layer is relatively stable, which we believe prevents oxidation of the aluminum (fig. S6), and the AlCl<sub>3</sub> and aqueous electrolyte provide an acidic internal environment that further stabilizes the ASEI, which together maintain a fresh Al surface and enable the operation of cells.

## Aqueous Al batteries with metal oxide cathodes

Building on the success of the TAI electrodes in facilitating reversible stripping and plating of Al in aqueous liquid electrolytes, we next explore applications of these electrodes and electrolytes in full-cell Al batteries. We here choose the well-studied MnO<sub>2</sub> for the cathode because it has a tunable structure and variable valence, and has been reported in multiple previous studies as a cathode candidate for high-capacity charge storage (25, 26). We use a hydrothermal method that enables facile synthesis of α-MnO<sub>2</sub> in a nanorod morphology (fig. S7). The one-dimensional nanostructures are advantageous because they should facilitate fast charge transport in the cathode. In cells using pristine Al, the electrochemical process is generally very sluggish, but an aqueous electrolyte based on 1 m Al(CF<sub>3</sub>SO<sub>3</sub>)<sub>3</sub> exhibits good reversibility with the MnO<sub>2</sub> cathode (fig. S8). The cell polarization is high (ca. 0.8 V), however, implying that there are large inefficiencies during the charge and discharge processes at the electrodes. The corresponding results for cells based on TAI electrodes are reported in Fig. 3A and fig. S9. It is seen that these cells exhibit both high reversibility and low levels of polarization. For example, TAl-MnO $_2$  cells that use a 2 m Al(CF $_3$ SO $_3$ ) $_3$  electrolyte display a high specific capacity of 380 mAh/g and an average discharge potential of ~1.3 V, corresponding to an energy density of approximately 500 Wh/kg, based on the mass of MnO $_2$ . A more practical estimate of the specific energy of the cell, based on the full cell mass [i.e., the MnO $_2$  content of the cathode ~70 weight % (wt %)], the Al anode (estimated to be 100% in excess), and other electrochemically inactive cell components (estimated to comprise 20 wt % of the cell mass), is 235 Wh/kg. The important role that the interface formed on Al in the AlCl $_3$ -IL melt plays in facilitating Al stripping processes is further confirmed by the galvanostatic intermittent titration technique (GITT) (fig. S10).

To understand the electrochemical reactions and charge transport processes at the MnO<sub>2</sub> cathode, we performed cyclic voltammetry (CV) measurements at different scan rates (Fig. 3B). Of particular interest is how/why the bulky Al<sup>3+</sup> ions in an aqueous solution are able to reversibly access the  $\alpha$ -MnO<sub>2</sub> electrode. One major reduction peak (located at about 1.2 to 1.4 V) and one oxidation peak (located at about 1.5 to 1.9 V) are observed at all of scan rates. The peak current for both the reduction and oxidation peaks follows an obvious linear relationship with the square root of the scan rate (see inset to Fig. 3B), indicating that the electrode reactions are Faradaic and that transport at the MnO<sub>2</sub> electrode is

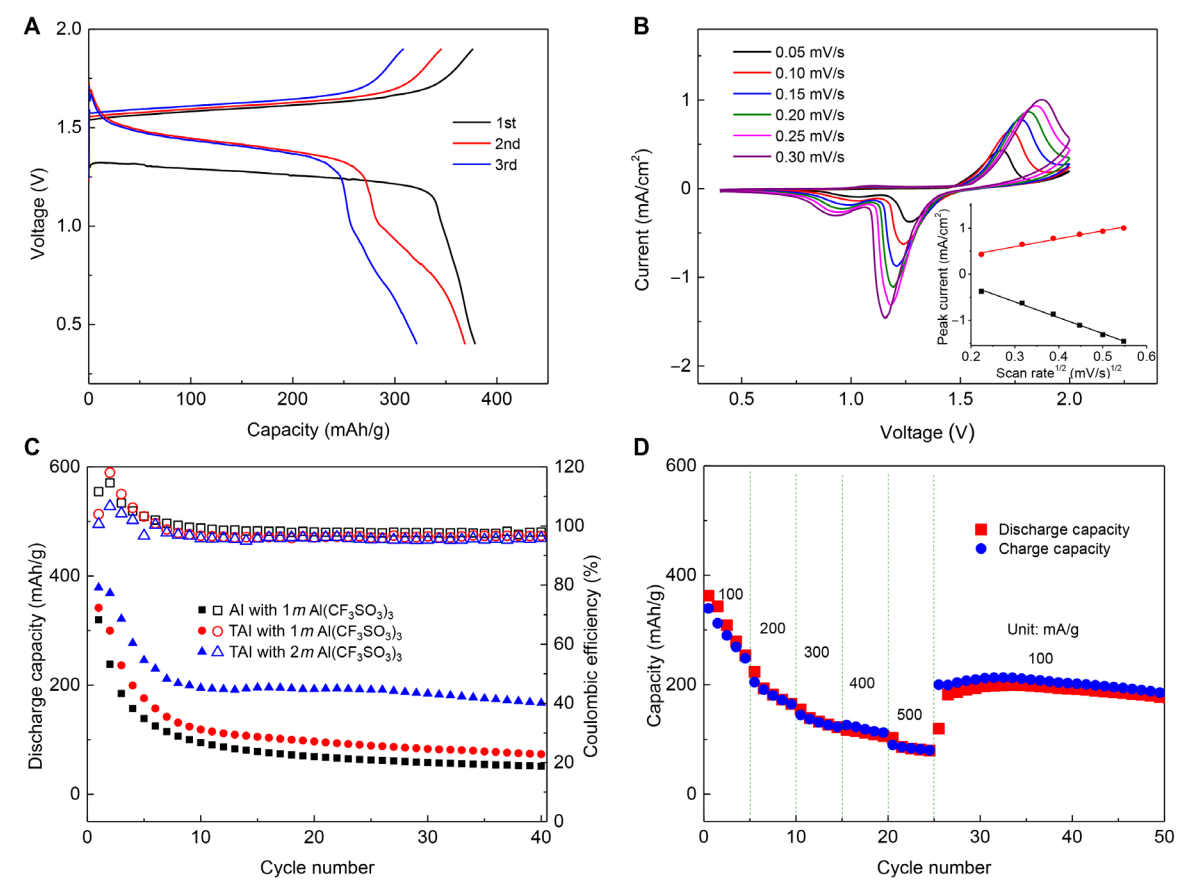


Fig. 3. Electrochemical performance of aqueous rechargeable Al batteries using  $\alpha$ -MnO<sub>2</sub> as the cathode. (A) Galvanostatic discharge/charge curves of aqueous Al batteries at a current density of 100 mA/g (MnO<sub>2</sub>) using TAI and electrolyte of 2 m Al(CF<sub>3</sub>SO<sub>3</sub>)<sub>3</sub> in H<sub>2</sub>O. (B) CV diagram at scanning rates of 0.05, 0.10. 0.15, 0.20, 0.25, 0.30, and 0.35 mV/s. The inset is the linear fit of the square root of the scan rate and the peak current. (C) Cycling performance of aqueous Al batteries using Al or TAI and electrolyte of 2 m or 1 m Al(CF<sub>3</sub>SO<sub>3</sub>)<sub>3</sub>. (D) Rate performance at different current densities using TAI and 2 m Al(CF<sub>3</sub>SO<sub>3</sub>)<sub>3</sub>.

under diffusion control. The results further show that TAl-MnO<sub>2</sub> cells based on the 2 m Al( $CF_3SO_3$ )<sub>3</sub> electrolyte exhibit the highest levels of reversibility and stable capacity retention after 40 cycles of charge and discharge at a rate of 100 mA/g, achieving a discharge capacity of 168 mAh/g (fig. S3C). Values of the coulombic efficiency in excess of 100% observed during the first few cycles are attributed to the partly irreversible reactions involved in forming favorable interphases at the cathode and anode of the cell. As shown in table S1, there is still a small amount of Al in the charging products, which causes the discharge capacity to slightly exceed the charge capacity for the first few cycles. All TAl-MnO<sub>2</sub> cells show some level of capacity fading, however, which we tentatively attribute to dissolution of low-valency Mn discharge products formed at the cathode and the partly irreversible reaction at the beginning. A straightforward approach for simultaneously evaluating this hypothesis and for improving the capacity retention is to lower the thermodynamic driving force for the dissolution process by introducing a finite concentration of low-valency Mn salt into the electrolyte (27, 28). Here, we introduced 0.1 m Mn(CF<sub>3</sub>SO<sub>3</sub>)<sub>2</sub> salt to the electrolyte and observed substantial improvements in both the discharge capacity and capacity retention, resulting in TAl-MnO<sub>2</sub> cells that can be reversibly cycled for more than 100 cycles at a rate of

 $200\,mA/g$  (fig. S11). The cells also show promising high-rate performance, achieving a capacity close to  $100\,mAh/g$  at a current density of 500mA/g (figs. S3D and S12).

## The mechanism of aqueous Al batteries

Further insights into the electrochemical processes at the cathode can be obtained from a combination of x-ray diffraction (XRD), electron microscopy, and spectroscopic analysis. XRD patterns obtained for cells at different stages of cycling (Fig. 4A) show that the electrode structure is highly stable after the recharge process. After full discharge, the peaks of MnO<sub>2</sub> remain and several new x-ray peaks are observed at the cathode (fig. S13A), which cannot be assigned to any known Mn-based product. These peaks can be eliminated by washing the cathode with water (fig. S13B), indicating that the compound(s) responsible is water soluble. Analysis of the cathode by SEM shows that the MnO<sub>2</sub> nanorods are well covered with a compact, smooth coating after the discharge (fig. S14, A and B). Charging the cell results in the disappearance of the coating from the nanorod structure (fig. S14, C and D), indicating that the material is created by an electrochemical process at the MnO<sub>2</sub> cathode and that its formation/removal reactions are reversible. Further EDX spectroscopic analysis of the cathode (fig. S15 and

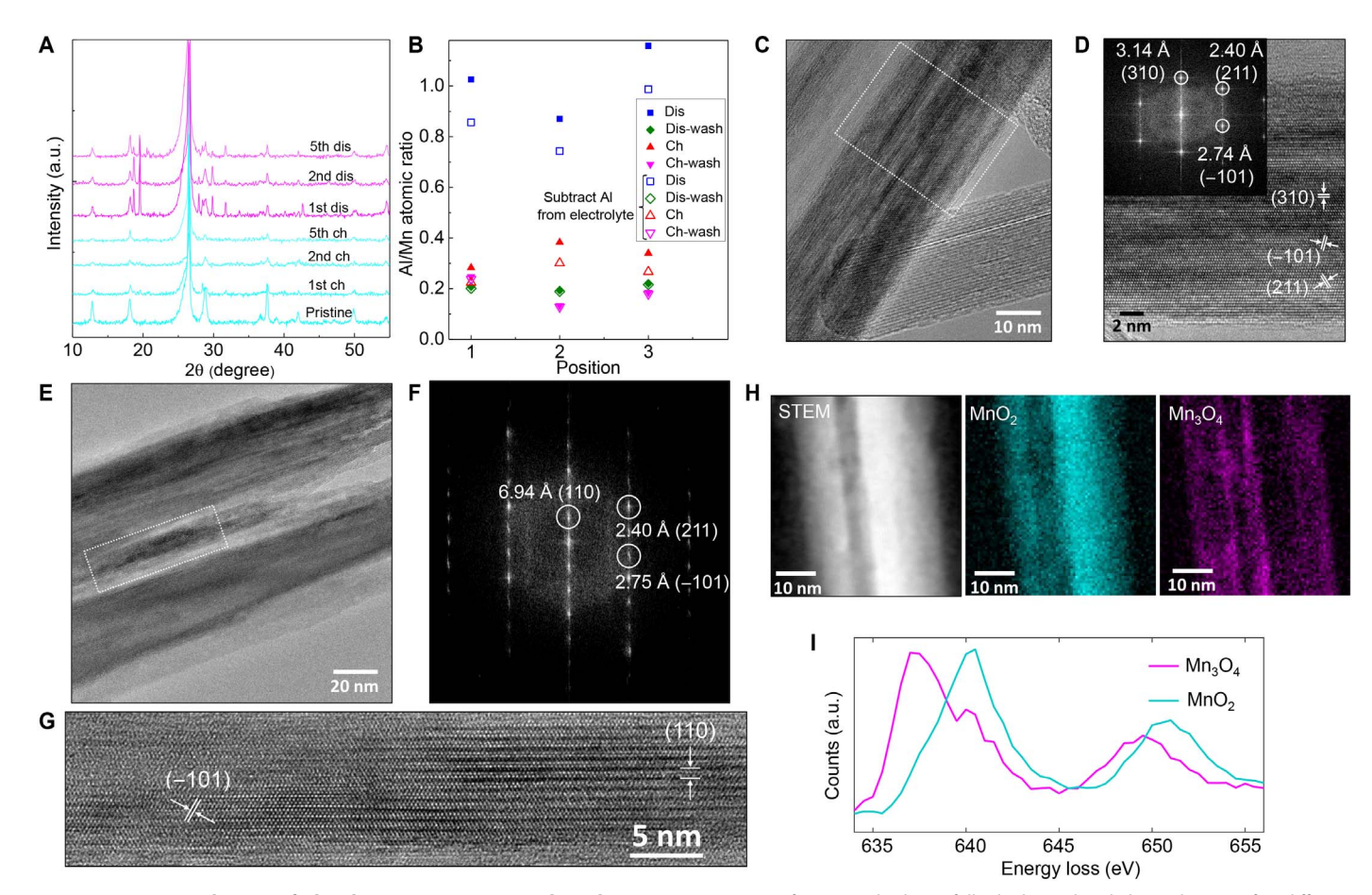


**Fig. 4. Reaction mechanism of AI with** α-**MnO**<sub>2</sub> **in aqueous electrolyte.** (**A**) XRD patterns of MnO<sub>2</sub> cathodes at fully discharged and charged states after different numbers of cycle. (**B**) Al/Mn ratio by SEM-EDX analysis of cathode after the first discharge and charge (washed or unwashed; include or subtract AI from electrolyte). (**C**) High-resolution TEM image and (**D**) corresponding enlarged view of pristine MnO<sub>2</sub> cathode. The inset in (D) is the fast Fourier transform (FFT) of the image. (**E**) High-resolution TEM image, (**F**) FFT pattern, and (**G**) corresponding enlarged part of discharged MnO<sub>2</sub> cathode. (**H**) Annular dark-field scanning transmission electron microscope (STEM) image and corresponding EELS mapping of fully discharged MnO<sub>2</sub> cathode nanorod. (**I**) The two Mn valence states present were likely MnO<sub>2</sub> and Mn<sub>3</sub>O<sub>4</sub>, as determined by multivariate curve resolution analysis of the Mn L<sub>2,3</sub> edge.

table S1) indicates that the discharge product displays a much higher Al/ Mn atomic ratio than the charge product (Fig. 4B). This analysis also shows that the Al component is diminished after washing the electrode with water, indicating that the Al-rich discharge product is the soluble phase. Transmission electron microscopy (TEM) analysis of the pristine MnO<sub>2</sub> shows that the nanorod structure has a high level of crystallinity and that α-MnO<sub>2</sub> is present (Fig. 4, C and D). The MnO<sub>2</sub> retains its nanorod structure after discharge (fig. S16). Using high-resolution TEM analysis, we confirmed that the nanorod structure is crystalline MnO<sub>2</sub> (Fig. 4, E to G). No obvious Al signal is detected in the discharged MnO<sub>2</sub> nanorod by electron energy-loss spectroscopy (EELS). However, EELS mapping reveals that a low-valence Mn material (most likely Mn<sub>3</sub>O<sub>4</sub>) is present on the nanorod surface (Fig. 4, H and I) (29). XPS results show that the proportion of reduced Mn valence states is largely increased in discharged product (fig. S17). These results can be united with previous analyses of electrochemical transitions at  $\alpha$ -MnO<sub>2</sub> in other metal batteries (28, 30) to propose the following reaction mechanism for our aqueous Al-MnO2 electrochemical cells

Anode: Al 
$$-3e^{-} \rightleftharpoons Al^{3+}$$
  
Cathode:  $3H_2O \rightleftharpoons 3H^+ + 3OH^-$   
 $xMnO_2 + 3e^- + 3H^+ \rightleftharpoons yMnO_{(2-\frac{3}{2y})} @(x-y)MnO_2 +$   
 $\frac{3}{2}H_2O \ (1.5 < y < 3)$   
 $Al^{3+} + 3OH^- + [ele] + zH_2O \rightleftharpoons Al(OH)_3[ele]zH_2O$   
Overall:  $Al + xMnO_2 + (\frac{3}{2} + z)H_2O + [ele] \rightleftharpoons yMnO_{(2-\frac{3}{2y})}$   
 $@(x-y)MnO_2 + Al(OH)_3[ele]zH_2O$ 

The major reaction happening in the Al cells can therefore be thought to involve two major steps. The stripping of aluminum at the anode reduces MnO2, which causes the appearance of the amorphous layer on MnO2. The resultant discharge product of MnO2 displays a core/shell-type morphology, in which the amorphous shell consists of low-valence manganese oxide and the crystal core still retains the structure of the  $\alpha\text{-MnO}_2$  rods. In addition, the Al ions stripped from the anode may react with electrolyte and form a complicated product rich in Al and electrolyte components.

#### **DISCUSSION**

Our results demonstrate that a good SEI on Al provides a key step toward enabling high-capacity aqueous aluminum batteries. In particular, we find that replacing the natural passivating oxide film on Al with an IL-rich ASEI facilitates a reversible stripping and plating process at a metallic Al anode. By coupling these anodes with a simple manganese oxide cathode, the aqueous Al batteries, we further find that the resultant Al cells deliver an energy density up to 500 Wh/kg. Our studies therefore open a new path toward achieving high-capacity, low-cost, and safe aqueous batteries.

## **MATERIALS AND METHODS**

## Preparation of electrolyte

The AlCl<sub>3</sub>-IL electrolyte was synthesized in Ar-filled glove box (Inert Inc.) by slowly adding AlCl<sub>3</sub> (99.99%; Sigma-Aldrich) into [EMIm]Cl (>95%; Sigma-Aldrich) (AlCl<sub>3</sub>/[EMIm]Cl is 1.3:1). The aqueous electrolyte was prepared by dissolving corresponding mole salts into water.

For example, 10, 20, 30, and 50 mM Al(CF<sub>3</sub>SO<sub>3</sub>)<sub>3</sub> (99%; Alfa Aesar) were added to 10 ml of water to prepare the Al(CF<sub>3</sub>SO<sub>3</sub>)<sub>3</sub> electrolyte with concentrations of 1 m, 2 m, 3 m, and 5 m, respectively. Al<sub>2</sub>(SO<sub>4</sub>)<sub>3</sub> aqueous electrolyte (1 m) was prepared by adding 10 mM Al<sub>2</sub>(SO<sub>4</sub>)<sub>3</sub>·18H<sub>2</sub>O (laboratory grade, Aldon Corp.) to 10 ml of water.

## Preparation of $\alpha$ -MnO<sub>2</sub> nanorod

 $\alpha\text{-MnO}_2$  was prepared by a traditional hydrothermal method (31). In a typical experiment, 5 mM KMnO $_4$  was first dissolved into the solution of 24 ml of 1.0 M HCl. Then, the volume was filled to 70 ml by adding distilled water. After stirring for half an hour, the solution was transferred to a 100-ml hydrothermal reactor. The reactor was placed at 140°C and reacted for 18 hours. The solution was then filtered to obtain the solid product, which was washed by distilled water and ethanol for three times. The MnO $_2$  nanorods were synthesized after drying in a vacuum oven at 80°C.

# Preparation of Al anode

Al foil (0.25 mm thick, annealed; 99.99%; Alfa Aesar) was used as the source of anode. Before using, the Al foil, which was used as the common Al anode, was polished with sand paper until the surface shined with metallic luster. For IL-treated Al anode (TAl), the common Al was impregnated in the IL electrolyte for more than 1 day. Then, the wet surface was cleaned before using for characterization and assembling any types of batteries.

## Preparation of Al batteries

All metal Al-based aqueous batteries [symmetric Al batteries, Al-carbon fiber paper batteries, and Al-MnO<sub>2</sub> batteries] were assembled in atmospheric environment using a coin 2032-type battery model. Glass fiber or Celgard 3501 was used as separator. To prepare MnO<sub>2</sub> cathodes, MnO<sub>2</sub>, Super P, and polyvinylidene fluoride with a weight ratio of 70:20:10 were mixed with *N*-methylpyrone (NMP) and painted on carbon fiber paper or Ti foil. The cathode was obtained after removing NMP at 80°C overnight. The areal loading of MnO<sub>2</sub> is about 2 mg/cm<sup>2</sup>.

## Characterizations of materials and batteries

dc ionic conductivity and EIS were measured using a Novocontrol broadband dielectric/impedance spectrometer. Field-emission SEM (FESEM) images of MnO $_2$  cathode and Al anode were obtained using a Leo 1550 Keck FESEM, in which EDX analysis was also carried out with a Bruker EDX detector. The XRD pattern of  $\alpha$ -MnO $_2$  cathodes during electrochemical reaction was taken with a Rigaku x-ray diffractometer. ATR-FTIR spectra of different electrolytes were obtained using a Bruker Hyperion FTIR spectrometer. XPS SSX-100 was applied to study the chemistry information of SEI on the Al surface and MnO $_2$  cathodes. Galvanostatic measurements of Al batteries were performed using Neware battery testers at room temperature. CV diagram was performed on an electrochemical workstation of CH 600E. TEM images were obtained from the FEI Titan Themis CryoS/TEM, in which EELS spectra were obtained using a Gatan GIF Tridiem energy filter.

# SUPPLEMENTARY MATERIALS

Supplementary material for this article is available at http://advances.sciencemag.org/cgi/content/full/4/11/eaau8131/DC1

Fig. S1. The SEM-EDX mapping spectra on the top view of TAL.

Fig. S2. Rate performance of symmetric Al batteries using TAI and electrolyte of 1 m Al(CF<sub>3</sub>SO<sub>3</sub>)<sub>3</sub> in water

Fig. S3. Symmetric Al battery performance using Al or TAl coupled with organic electrolyte.

- Fig. S4. The CV diagrams of Al-carbon fiber paper batteries.
- Fig. S5. ATR-FTIR spectra of different electrolytes.
- Fig. S6. Cross-sectional SEM image of TAI anode and corresponding EDX mapping after cycling in symmetric batteries.
- Fig. S7. SEM characterizations of MnO<sub>2</sub> nanorod.
- Fig. S8. Galvanostatic discharge/charge curves of aqueous Al batteries using common Al anode. Fig. S9. Electrochemical properties of Al-MnO $_2$  batteries using TAl anode–, Al(CF $_3$ SO $_3$ ) $_3$ -, and Al $_2$ (SO $_4$ ) $_3$ -based aqueous electrolyte.
- Fig. S10. GITT profiles of Al-MnO<sub>2</sub> batteries.
- Fig. S11. Cycling performance comparisons with or without Mn(CF<sub>3</sub>SO<sub>3</sub>)<sub>2</sub> addition at current density of 200 mA/a.
- Fig. S12. Galvanostatic discharge/charge curves at different current densities.
- Fig. S13. XRD patterns of MnO<sub>2</sub> electrodes under different situations.
- Fig. S14. SEM images of MnO<sub>2</sub> electrode.
- Fig. S15. SEM images and selected positions for EDX studies.
- Fig. S16. TEM images of MnO<sub>2</sub> electrodes.
- Fig. S17. XPS  $Mn_{2p3/2}$  spectra of pristine  $MnO_2$ , fully discharged  $MnO_2$  cathode, and fully charged  $MnO_2$  cathode.

Table S1. EDX analysis of points in fig. S15.

References (32-36)

#### **REFERENCES AND NOTES**

- B. Dunn, H. Kamath, J.-M. Tarascon, Electrical energy storage for the grid: A battery of choices. Science 334, 928–935 (2011).
- M. S. Whittingham, Ultimate limits to intercalation reactions for lithium batteries. Chem. Rev. 114, 11414–11443 (2014).
- U.S. Environmental Protection Agency, Inventory of U.S. Greenhouse Gas Emissions and Sinks (1990-2016) (U.S. Environmental Protection Agency, 2018).
- J. Muldoon, C. B. Bucur, T. Gregory, Quest for nonaqueous multivalent secondary batteries: Magnesium and beyond. Chem. Rev. 114, 11683–11720 (2014).
- G. A. Elia, K. Marquardt, K. Hoeppner, S. Fantini, R. Lin, E. Knipping, W. Peters, J.-F. Drillet, S. Passerini, R. Hahn, An overview and future perspectives of aluminum batteries. *Adv. Mater.* 28, 7564–7579 (2016).
- W. I. Al Sadat, L. A. Archer, The O<sub>2</sub>-assisted Al/CO<sub>2</sub> electrochemical cell: A system for CO<sub>2</sub> capture/conversion and electric power generation. Sci. Adv. 2, e1600968 (2016).
- 7. Y. Liu, Q. Sun, W. Li, K. R. Adair, J. Li, X. Sun, A comprehensive review on recent progress in aluminum–air batteries. *Green Energy Environ.* **2**, 246–277 (2017).
- D. Peramunage, R. Dillon, S. Licht, Investigation of a novel aqueous aluminum/sulfur battery. J. Power Sources 45, 311–323 (1993).
- 9. N. Jayaprakash, S. K. Das, L. A. Archer, The rechargeable aluminum-ion battery. *Chem. Commun.* **47**, 12610–12612 (2011).
- M.-C. Lin, M. Gong, B. Lu, Y. Wu, D.-Y. Wang, M. Guan, M. Angell, C. Chen, J. Yang, B.-J. Hwang, H. Dai, An ultrafast rechargeable aluminium-ion battery. *Nature* 520, 325–328 (2015).
- 11. H. Chen, H. Xu, S. Wang, T. Huang, J. Xi, S. Cai, F. Guo, Z. Xu, W. Gao, C. Gao, Ultrafast all-climate aluminum-graphene battery with quarter-million cycle life. *Sci. Adv.* **3**, eaao7233 (2017).
- G. Cohn, L. Ma, L. A. Archer, A novel non-aqueous aluminum sulfur battery. J. Power Sources 283, 416–422 (2015).
- T. Gao, X. Li, X. Wang, J. Hu, F. Han, X. Fan, L. Suo, A. J. Pearse, S. B. Lee, G. W. Rubloff, K. J. Gaskell, M. Noked, C. Wang, A rechargeable Al/S battery with an ionic-liquid electrolyte. *Angew. Chem. Int. Ed.* 55, 9898–9901 (2016).
- H. Tian, S. Zhang, Z. Meng, W. He, W.-Q. Han, Rechargeable aluminum/iodine battery redox chemistry in ionic liquid electrolyte. ACS Energy Lett. 2, 1170–1176 (2017).
- Y. Hu, B. Luo, D. Ye, X. Zhu, M. Lyu, L. Wang, An innovative freeze-dried reduced graphene oxide supported SnS<sub>2</sub> cathode active material for aluminum-ion batteries. *Adv. Mater.* 29, 1606132 (2017)
- L. Geng, J. P. Scheifers, C. Fu, J. Zhang, B. P. T. Fokwa, J. Guo, Titanium sulfides as intercalation-type cathode materials for rechargeable aluminum batteries. ACS Appl. Mater. Interfaces 9, 21251–21257 (2017).
- L. Geng, G. Lv, X. Xing, J. Guo, Reversible electrochemical intercalation of aluminum in Mo<sub>6</sub>S<sub>8</sub>. Chem. Mater. 27, 4926–4929 (2015).
- A. VahidMohammadi, A. Hadjikhani, S. Shahbazmohamadi, M. Beidaghi, Two-dimensional vanadium carbide (MXene) as a high-capacity cathode material for rechargeable aluminum batteries. ACS Nano 11, 11135–11144 (2017).
- P. Verma, P. Maire, P. Novák, A review of the features and analyses of the solid electrolyte interphase in Li-ion batteries. *Electrochim. Acta* 55, 6332–6341 (2010).
- X.-B. Cheng, R. Zhang, C.-Z. Zhao, Q. Zhang, Toward safe lithium metal anode in rechargeable batteries: A review. Chem. Rev. 117, 10403–10473 (2017).

- H. Wang, S. Gu, Y. Bai, S. Chen, N. Zhu, C. Wu, F. Wu, Anion-effects on electrochemical properties of ionic liquid electrolytes for rechargeable aluminum batteries. *J. Mater. Chem. A* 3, 22677–22686 (2015).
- L. M. Suo, O. Borodin, T. Gao, M. Olguin, J. Ho, X. L. Fan, C. Luo, C. Wang, K. Xu, "Water-in-salt" electrolyte enables high-voltage aqueous lithium-ion chemistries. Science 350, 938–943 (2015).
- R.-S. Kühnel, D. Reber, C. Battaglia, A high-voltage aqueous electrolyte for sodium-ion batteries. ACS Energy Lett. 2, 2005–2006 (2017).
- Y. Yamada, K. Usui, K. Sodeyama, S. Ko, Y. Tateyama, A. Yamada, Hydrate-melt electrolytes for high-energy-density aqueous batteries. *Nat. Energy* 1, 16129 (2016).
- G. G. Yadav, J. W. Gallaway, D. E. Turney, M. Nyce, J. Huang, X. Wei, S. Banerjee, Regenerable Cu-intercalated MnO<sub>2</sub> layered cathode for highly cyclable energy dense batteries. *Nat. Commun.* 8, 14424 (2017).
- 26. L. M. Housel, L. Wang, A. Abraham, J. Huang, G. D. Renderos, C. D. Quilty, A. B. Brady, A. C. Marschilok, K. J. Takeuchi, E. S. Takeuchi, Investigation of  $\alpha$ -MnO $_2$  tunneled structures as model cation hosts for energy storage. *Acc. Chem. Res.* **51**, 575–582 (2018).
- N. Zhang, F. Cheng, J. Liu, L. Wang, X. Long, X. Liu, F. Li, J. Chen, Rechargeable aqueous zinc-manganese dioxide batteries with high energy and power densities. *Nat. Commun.* 8, 405 (2017).
- H. Pan, Y. Shao, P. Yan, Y. Cheng, K. S. Han, Z. Nie, C. Wang, J. Yang, X. Li, P. Bhattacharya, K. T. Mueller, J. Liu, Reversible aqueous zinc/manganese oxide energy storage from conversion reactions. *Nat. Energy* 1, 16039 (2016).
- B. Gilbert, B. H. Frazer, A. Belz, P. G. Conrad, K. H. Nealson, D. Haskel, J. C. Lang, G. Srajer, G. De Stasio, Multiple scattering calculations of bonding and X-ray absorption spectroscopy of manganese oxides. J. Phys. Chem. A 107, 2839–2847 (2003).
- T. S. Arthur, R. Zhang, C. Ling, P.-A. Glans, X. Fan, J. Guo, F. Mizuno, Understanding the electrochemical mechanism of K-αMnO<sub>2</sub> for magnesium battery cathodes. ACS Appl. Mater. Interfaces 6, 7004–7008 (2014).
- J. Luo, H. T. Zhu, H. M. Fan, J. K. Liang, H. L. Shi, G. H. Rao, J. B. Li, Z. M. Du, Z. X. Shen, Synthesis of single-crystal tetragonal α-MnO<sub>2</sub> nanotubes. *J. Phys. Chem. C* 112, 12594–12598 (2008).
- W. W. Rudolph, R. Mason, Study of aqueous Al<sub>2</sub>(SO<sub>4</sub>)<sub>3</sub> solution under hydrothermal conditions: Sulfate ion pairing, hydrolysis, and formation of hydronium alunite. *J. Solution Chem.* 30, 527–548 (2001).
- S. A. Suthanthiraraj, B. J. Paul, Investigation on structural characteristics of PVDF-AgCF<sub>3</sub>SO<sub>3</sub>-Al<sub>2</sub>O<sub>3</sub> nanocomposite solid polymer electrolyte system. *Ionics* 13, 365–368 (2007).
- H. W. Nesbitt, D. Banerjee, Interpretation of XPS Mn(2p) spectra of Mn oxyhydroxides and constraints on the mechanism of MnO<sub>2</sub> precipitation. Am. Mineral. 83, 305–315 (1998).
- Q. Tang, L. Jiang, J. Liu, S. Wang, G. Sun, Effect of surface manganese valence of manganese oxides on the activity of the oxygen reduction reaction in alkaline media. ACS Catal. 4, 457–463 (2014).
- Y. Yuan, A. Nie, G. M. Odegard, R. Xu, D. Zhou, S. Santhanagopalan, K. He, H. Asayesh-Ardakani, D. D. Meng, R. F. Klie, C. Johnson, J. Lu, R. Shahbazian-Yassar, Asynchronous crystal cell expansion during lithiation of K<sup>+</sup>-stabilized α-MnO<sub>2</sub>. Nano Lett. 15, 2998–3007 (2015).

## Acknowledgments

Funding: This work was supported by the Department of Energy Basic Energy Sciences Program through award DE-SC0016082 and by the Advanced Research Projects Agency-ARPA-E through award DE-AR-0000750. M.J.Z. and L.F.K. acknowledge support by the NSF (DMR-1654596). This work made use of the Cornell Center for Materials Research (CCMR) Shared Facilities with funding from the NSF MRSEC program (DMR-1719875). The FEI Titan Themis 300 was acquired through NSF MRI-1429155, with additional support from Cornell University, the Weill Institute, and the Kavli Institute at Cornell. Author contributions: Q.Z. and L.A. conceived and designed this work. Q.Z., W.A.S., and J.Z. prepared and characterized the aqueous Al batteries. M.J.Z. and L.F.K. conducted the TEM analysis. All authors contributed to the data analysis. L.A. directed the research. Competing interests: L.A. is a founder and member of the board of directors of NOHMs Technologies. This company develops and commercializes electrolytes for lithium-ion and lithium-sulfur battery technology. The authors declare no other competing interests. Data and materials availability: All data needed to evaluate the conclusions in the paper are present in the paper and/or the Supplementary Materials. Additional data related to this paper may be requested from the authors.

Submitted 17 July 2018 Accepted 31 October 2018 Published 30 November 2018 10.1126/sciady.aau8131

Citation: Q. Zhao, M. J. Zachman, W. I. Al Sadat, J. Zheng, L. F. Kourkoutis, L. Archer, Solid electrolyte interphases for high-energy aqueous aluminum electrochemical cells. *Sci. Adv.* 4, eaau8131 (2018).



## Solid electrolyte interphases for high-energy aqueous aluminum electrochemical cells

Qing Zhao, Michael J. Zachman, Wajdi I. Al Sadat, Jingxu Zheng, Lena F. Kourkoutis and Lynden Archer

Sci Adv 4 (11), eaau8131. DOI: 10.1126/sciadv.aau8131

ARTICLE TOOLS http://advances.sciencemag.org/content/4/11/eaau8131

SUPPLEMENTARY MATERIALS http://advances.sciencemag.org/content/suppl/2018/11/26/4.11.eaau8131.DC1

REFERENCES This article cites 35 articles, 5 of which you can access for free http://advances.sciencemag.org/content/4/11/eaau8131#BIBL

PERMISSIONS http://www.sciencemag.org/help/reprints-and-permissions

Use of this article is subject to the Terms of Service